Progress In Electromagnetics Research C, Vol. 118, 263–275, 2022

Miniaturized Quad-Port UWB-MIMO Antenna with Band-Notched Characteristics at 5 GHz

Qasim H. Kareem[1, 2, *] and Malik J. Farhan[1]

Abstract—Small footprint of the multi-input-multi-output (MIMO) antenna is extremely desirable for space-constrained ultra-wideband (UWB) communication systems. Compact MIMO antennas with improved isolation and wide operating bandwidth are the significant subject of the work. Therefore, this paper presents a miniaturized four-port polarization diversity UWB-MIMO antenna operating in the frequency range of 3.1–12 GHz with band-notched characteristics. Four octagon-shaped radiating elements with a common ground are placed orthogonal to each other for good isolation. Band rejection features between 4.5 and 5.5 GHz were achieved by including an open-ended slot at the upper edge of the octagonal-shaped antenna. The MIMO antenna was etched on a low-cost $32.3 \times 32.3 \times 0.8\,\text{mm}^3$ FR-4 dielectric substrate. The antenna radiates in a quasi-omnidirectional pattern on the H-plane throughout the operational bandwidth, with higher than 15 dB isolation, low envelope correlation, and high antenna gain. As a result, this antenna is well suited for diverse applications and portable devices.

1. INTRODUCTION

Ultra-wideband (UWB) systems have been in demand during the past decade because of wide impedance bandwidth, good time-domain resolution, and high-speed data rate. The Federal Communication Commission (FCC) has assigned the 3.1–10.6 GHz frequency range to UWB applications [1]. Compact, low-profile, simple-to-integrate, and omnidirectional antennas are made for this technology to make it easier to use with devices of small physical size [2]. UWB's power spectrum is constrained by multipath fading in dense propagation settings, making MIMO the superior choice for increasing spectral efficiency [3]. The close spacing of the antennas, particularly in portable devices, unavoidably results in significant mutual coupling between the radiators. In recent years, various solutions have been proposed to reduce the impacts of mutual coupling in UWB-MIMO antennas [4–15]. Methods include a short ground strip and two long protruding stubs on the ground [4], adding a T-shaped decoupling stub structure [5, 6], locating neutralization line above ground plane [7], etching a line and a T-shaped slot on the ground plane [8], placing a Y-shaped slot that is cut at the bottom center of the common ground plane [9], protruding ground structure [10], using orthogonal arrangements of radiators with protruded ground plane [11], adding electromagnetic bandgap (EBG) [12], hybrid techniques combining defected ground plane structures (DGS) and stubs [13], and using parasitic elements [14, 15].

While the antenna designs discussed in the preceding literature exhibited acceptable isolation, some were not small enough, and others were very complex. However, because UWB systems operate at such a wide bandwidth, they inevitably overlap with several narrowband wireless applications, such as worldwide interoperability for microwave access (WiMAX) and wireless local area network (WLAN).

As a result, compact antennas with band-notch properties are required to ensure the reliability of UWB communication. Several strategies have been devised to create a compact UWB-MIMO antenna

Received 20 January 2022, Accepted 17 February 2022, Scheduled 3 March 2022

* Corresponding author: Qasim Hadi Kareem Al-Gertany (qasim.hadi2017@gmail.com).

[1] Electrical Engineering Department, Mustansiriyah University, Baghdad, Iraq. [2] Computer Engineering, Al-Farabi University College, Baghdad, Iraq.

with band-notch characteristics that can be used throughout the UWB spectrum [16–27]. A four-port UWB-MIMO antenna with dual polarization is proposed in [16]. Perpendicular taper microstrip feeding techniques are used to provide pentagonal radiators and lower the size of the MIMO system to $40 \times 40\,\text{mm}^2$. Although the MIMO antenna is comparable in size, the technique utilized to construct the antenna and reduce isolation to 15 dB is somewhat complicated. [17] presents a small quad-element octagonal fractal UWB-MIMO antenna. Koch fractal geometry's self-similar and space-filling features are exploited to miniaturize the design. The design employs grounded stubs to boost isolation to 17 dB at bandwidth 2–10.6 GHz. The antenna is $45 \times 45\,\text{mm}^2$ and has a quasi-omnidirectional radiating pattern. The common ground, however, is not connected. [18] shows two similar semicircular radiators with the symmetrical graded elliptical technique for UWB applications. Asymmetric curved-I shaped DGS is adopted, which increases the bandwidth from 1.99 to 10.02 GHz while decreasing mutual coupling to 13 dB. An 8.6 mm edge-to-edge spacing separates the two radiators to give exceptional variation with an overall optimum size of $50 \times 35\,\text{mm}^2$. [19] presents a dual-port Yagi MIMO antenna design for UWB applications based on loop excitation. The antenna's total size is reduced to $50 \times 80\,\text{mm}^2$ by implementing half of the driven loop element on either side of the substrate.

[20] proposes a four-port planar UWB-MIMO antenna placed on a substrate with a 3.1 to 10.6 GHz bandwidth. The substrate's two sides are symmetrical, with each side consisting of two radiators with partial ground planes to raise the isolation to 20 dB. The average gain value is 3.28 dBi, and the radiation pattern is omnidirectional. [21] presents a MIMO antenna for UWB applications that operates in the frequency range of 3.1 to 10.6 GHz. Two identical circular monopoles are created on a substrate. A planar decoupling design is added between the two antennas to create broad isolation. A central slot is engraved on the common ground to boost isolation to more than 31 dB. However, the antenna size is incompatible with compact portable devices. [22] illustrates a UWB-MIMO antenna with a triple-band rejection capability for two ports. The antenna rejects the frequencies of WLAN, WiMAX, and X-band. Electromagnetic Band Gap (EBG) structures aid in achieving band notches in WLAN and WiMAX bands. A notch in the X-band downlink satellite communication band comprises an EBG structure that is uniplanar plus-shaped. With an overall dimension of $64 \times 45\,\text{mm}^2$, decoupling strips and a slotted ground plane improve isolation to 15 dB. [23] presents a four-port UWB-MIMO antenna ideal for wireless body area network (WBAN) and wireless personal area network (WPAN) applications. The antenna has four microstrip feedlines with circular patches backed by circular stepped slots, with slot antennas arranged orthogonally to reduce the size to $36 \times 36\,\text{mm}^2$ and enhance isolation to 15 dB. The elements operate at 3.1–11.8 GHz with a realized gain of 3.5 dBi and no band-notch features. [24] proposes a four-port UWB-MIMO antenna that uses a neutralization-line technique to reduce mutual interaction between elements. A half-circle shaped disc is joined to a rectangle patch, and each of the two symmetrical antennas is connected to a neutralizing line to increase the isolation to -23 dB in the 3.5–10.1 GHz band. A compact four radiator reconfigurable design with reject demand bands ranging from 4.9 to 6.3 GHz and an impedance matching range (2–12 GHz) was presented in [25, 26]. Two radiators are arranged orthogonally to use the polarization variety and good isolation (> 17 dB) on a small substrate. Because of the angular placement and board cutting, the design is complex and challenging to manufacture. [27] presents four compact orthogonal MIMO antennas to improve isolation to -15 dB in the 3.1–10.6 GHz frequency band. The antenna size was lowered to $40 \times 40\,\text{mm}^2$ by altering the circular patch shape. However, the peak gain is 3 dBi, and the correlation coefficients are less than 0.4.

MIMO antenna design for the UWB region with notch band is progressing in light of the preceding brief literature review, but there is still a need for compact, band-notched characteristics, simple structure, broadband, and highly efficient antenna. As a result, our effort aims to design and analyze a compact quad-port band-notched UWB pattern diversity antenna with enriched isolation. Four antenna elements are symmetrically arranged and joined to a common ground. Compared to a two-element antenna, a four-element antenna considerably improves the quality of communication channels. Improved impedance bandwidth, high isolation, and improved diversity performance are all covered by the defective ground structure used to modify the ground plane. Furthermore, the slotted stubs are incorporated to reduce the mutual coupling between the radiating elements. The proposed design results in a compact size ($32.3 \times 32.3\,\text{mm}^2$) and the smallest UWB diversity antenna currently available.

2. GEOMETRY OF ANTENNA

2.1. UWB-Antenna Radiator

The designed unit cell of UWB-antenna is illustrated diagrammatically in Fig. 1. It comprises an octagonal resonating element fed by a microstrip line and a rectangle ground plane. A slot along the upper edge of the octagonal radiator with an open-ended slot is etched for notching the frequency band between 4.5 and 5.5 GHz. Impedance matching is improved by carving a U-shaped gap into the ground plane. The antenna is printed on a 0.8 mm thick sheet of FR-4 dielectric material with a relative permittivity of 4.3. The designed antenna is simulated, designed, and implemented using a computer simulation technology (CST) tool. Table 1 includes the dimensions of the octagonal monopole element.

Table 1. Dimensions of optimized parameters.

Parameters	Dim. (mm)	Parameters	Dim. (mm)	Parameters	Dim. (mm)	Parameters	Dim. (mm)
L	25	L_4	2.7	W_5	3.45	c_1	0.78
W	10.9	L_5	1.9	a_1	2.96	c_2, c_3	0.77
a, b, c	3.76	W_1	1.97	a_2	2.66	R_1	4.5
L_1	13	W_2	5.3	b_1	2.96	R_2	5.2
L_2	10.4	W_3	0.75	b_2	1.43	Ls	32.3
L_3	1	W_4	2.7	b_3	1.2	Ws	32.3

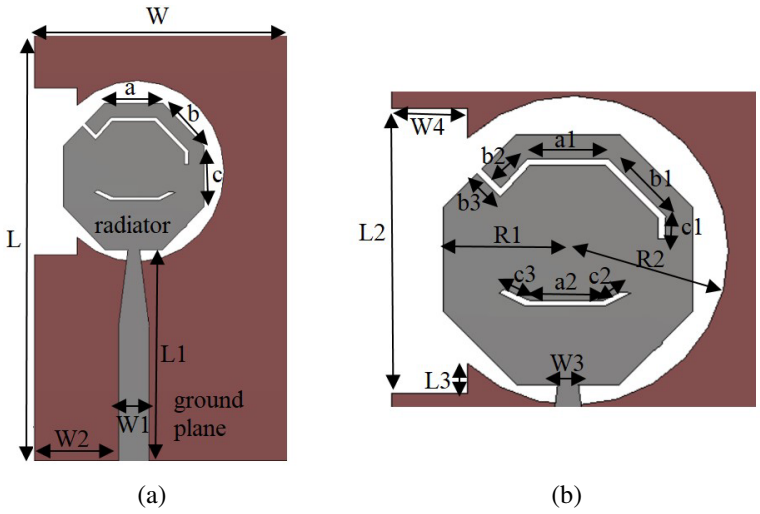

Figure 1. UWB-antenna structure: (a) Schematic layout; (b) Enlarge view of radiator.

Figure 2 illustrates the antenna design process. As shown, a 50-ohm microstrip line feeds an octagon-shaped radiator (step 1). Since the surface beneath the antenna radiating patch behaved as an imbalanced impedance, the radiator did not respond to any frequency band. An impedance match between the patch and feed line can be seen in Fig. 2(b) by carving a U-shaped gap into the ground plane beneath the radiator's edge (step 2). In Fig. 2(c), an open-ended slot is implanted into the antenna radiator to eliminate the 4.5–5.5 GHz interfering band, as illustrated in Fig. 3. As depicted in Fig. 2(d), the next step involves loading an additional slot opposite to step 3 onto the radiator to enhance impedance bandwidth (step 4) further. The resonant frequency of band-notched structure can

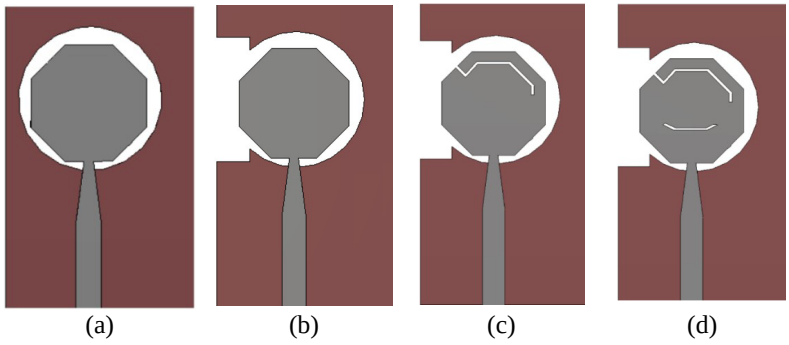

Figure 2. Octagonal-shaped antenna design, (a) Step-1, (b) Step-2, (c) Step-3, (d) Step-4.

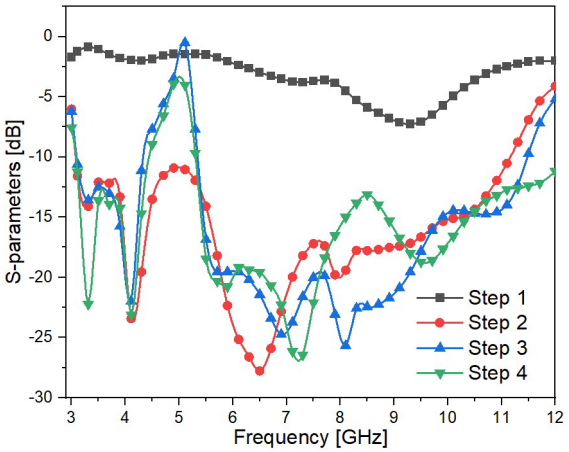

Figure 3. Reflection coefficient of the design steps (1–4).

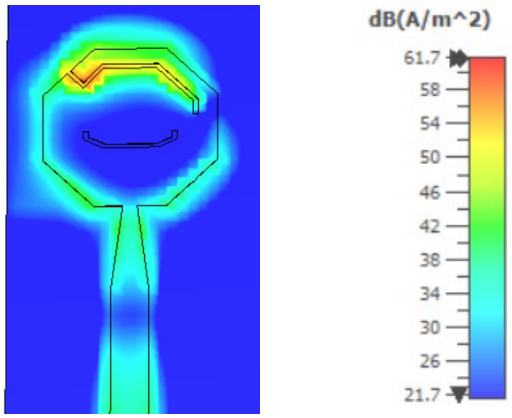

Figure 4. Surface current distribution at 5 GHz.

be calculated as:

$$f_{L_1} = \frac{C}{2L_1\sqrt{\varepsilon_{reff}}} \tag{1}$$

$$\varepsilon_{reff} = \frac{\varepsilon_r + 1}{2} \tag{2}$$

where f_{L_1} is the frequency of band-notched, L_1 the length of the band-notch slot, ε_r the substrate's dielectric constant, ε_{reff} the effective relative permittivity, and c the speed of light.

The slot length of band-notched is calculated as [28]

$$L_1 = 2\,(a_1 + b_1 + c_1 + b_2 + b_3) + W_{slot} \tag{3}$$

The band-notched frequency corresponds to the 5 GHz band, which has a slot length of 18.4 mm. Further, the MIMO antenna's band-notch response is validated by monitoring surface current distributions at 5 GHz. Fig. 4 illustrates the current distribution at 5 GHz with port-1 active and port-2 terminated with a 50 ohm matched load. A high current concentration is observed at this frequency along with the radiator's upper slot, resulting in the band's elimination. As a result, band-notched features are obtained by inserting an open-ended slot into the octagonal-radiating element.

2.2. Four-Port UWB-MIMO Antenna

The band-notched UWB-MIMO antenna's geometric layout is shown in Fig. 5, and its design parameters are listed in Table 1. The proposed design incorporates four identical octagon-shaped microstrip-line-fed

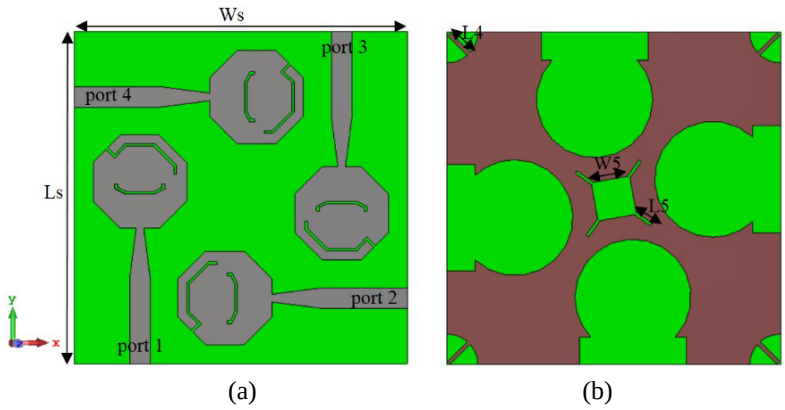

Figure 5. Geometric layout of the proposed design, (a) front and (b) back view.

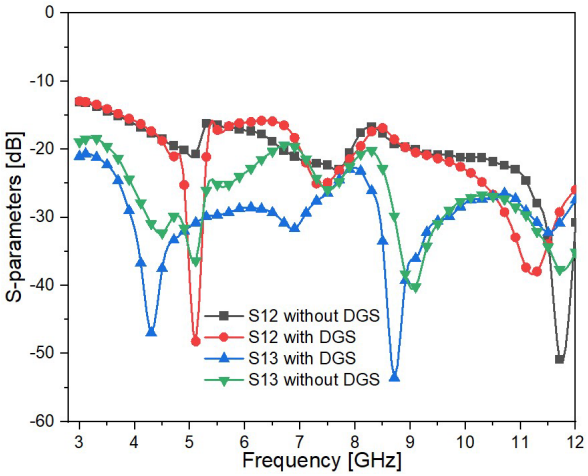

Figure 6. Transmission coefficients with DGS and without DGS.

radiators positioned in orthogonal orientations to provide diverse performance. The antenna feeding locations are denoted in the layout schematic as port1, port2, port3, and port4. The orthogonal radiation created between adjoining octagon-shaped elements results in increased isolation of more than -15 dB in the working band, causing a decrease in coupling between elements. However, because of the proximity of the resonating components, the weak mutual coupling is detected in Fig. 6 without DGS at lower frequencies, which can be minimized by incorporating ground surface decoupling devices. As a result, a DGS is added on the backside of the dielectric substrate between the antenna elements' ground patches to improve inter-element isolation. In addition, the square-slot constraint on the current emitted to adjacent excited elements increased the level of mutual coupling. The size and spacing of the circular slots were determined to get the optimal decoupling response by examining several simulations and the surface current distribution.

Additionally, these slots joined the ground of the four radiators to ensure that the antenna was designed with the same voltage. In a practical system, the resonating elements should share a common plane to interpret the signal intensity accurately; if not, the MIMO system will not operate efficiently [29, 30]. The antenna prototype is shown in Fig. 7, with a total size of $32.3 \times 32.3 \times 0.8\,\text{mm}^3$.

3. RESULTS AND DISCUSSIONS

A low-cost FR4 substrate with 4.3 dielectric permittivity and $\tan\delta = 0.025$ loss tangent is used to print the UWB-MIMO antenna. The size of the substrate is $32.3 \times 32.3\,\text{mm}^2$. S-parameters and the

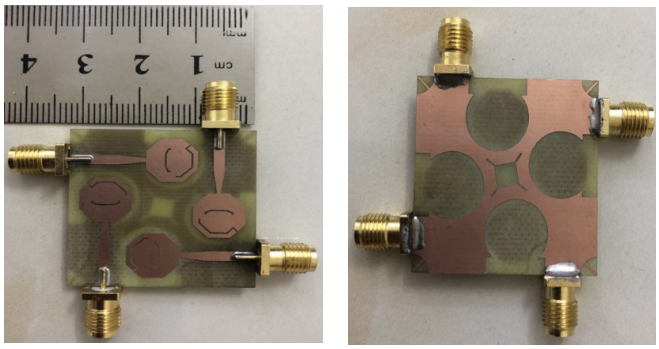

(a) (b)

Figure 7. A prototype of the proposed design, (a) front and (b) back view.

characteristics of the proposed geometry were simulated and measured using the CST Microwave Studio and KC901 vector network analyzer, respectively.

3.1. *S*-Parameters

Reflection coefficients is a significant metric for determining the antenna's operating bands. Fig. 8 illustrates the simulated and measured findings for return loss (S_{11}–S_{44}). The designed antenna provides a wider bandwidth of 3.1–12 GHz with a band-notched at 5 GHz. The outcomes are nearly identical at low frequencies, with minor exceptions at higher frequencies. This impact may be caused by the increased sensitivity of measured and constructed limitations to higher frequencies. For most portion, the actual reflection coefficient values match those simulated.

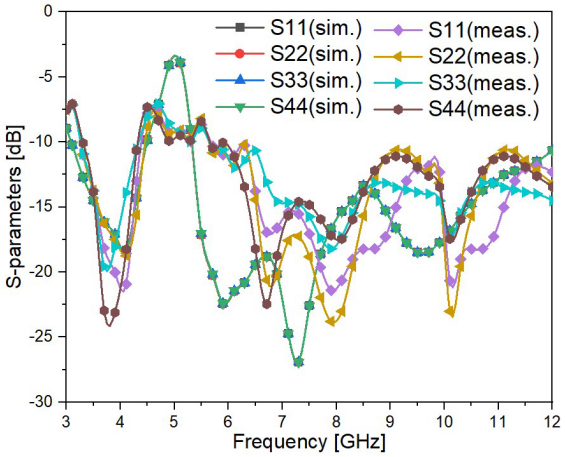

Figure 8. Simulated and measured results for the reflection coefficients.

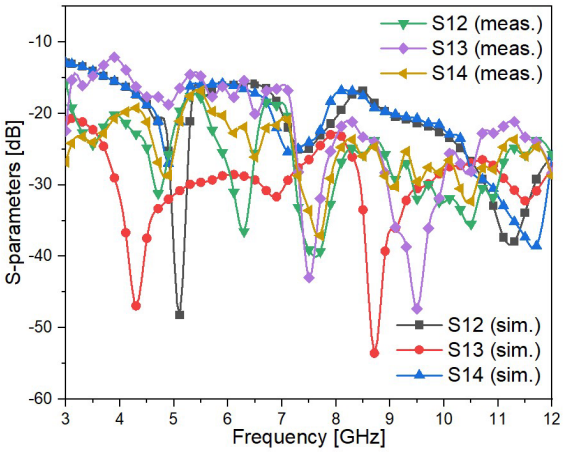

Figure 9. Simulated and measured results for the transmission coefficients.

The *S*-parameters, S_{12}, S_{13}, and S_{14}, are important for characterizing the mutual coupling of the MIMO system. Fig. 9 illustrates the measured and simulated findings for S_{12}, S_{13}, and S_{14}. These parameters are all less than 15 dB across the operational frequency spectrum. Due to the proposed antenna's symmetrical structure, S_{12} and S_{14} are nearly identical. Additionally, the measured values of S_{12}, S_{13}, and S_{14} are well within the range of the simulated values. A higher level of isolation is seen in the UWB-MIMO antenna, as evidenced by these findings.

3.2. MIMO Antenna Performance

The scattering matrix or S-parameters alone are insufficient to characterize a MIMO antenna completely. Therefore, the total active reflection coefficient (TARC) is introduced as a new parameter. It is the total reflected power ratio to the total incident power, expressed as a square root [31].

TARC can be expressed as follows for a MIMO antenna with N elements:

$$\Gamma_a^t = \frac{\sqrt{\sum_{i=1}^{N} |b_i|^2}}{\sqrt{\sum_{i=1}^{N} |a_i|^2}} \tag{4}$$

where a_i and b_i denote the incident and reflected signals at the antenna's ith port. Since a_i and b_i are associated with S-parameters, the TARC of an antenna can be described in terms of S-parameters. With a straightforward calculation based on the relationship,

$$[b] = [S][a] \tag{5}$$

The quad-port MIMO antenna system's TARC is expressed as [32]

$$\left(\Gamma_a^t\right)_{4-\text{port}} = \frac{\sqrt{\sum_{i=1}^{4} \left|S_{i1} + S_{i2}e^{j\theta_1} + S_{i3}e^{j\theta_2} + S_{i4}e^{j\theta_3}\right|^2}}{2} \tag{6}$$

where, θ is the phase of S-parameters, S_{ii} the return losses at tth port, and S_{ij} the mutual coupling between ith and jth ports.

Theoretical calculations obtain the TARC curves shown in Fig. 10 (Equation (6)). The TARC curves represent the MIMO antenna system's effective bandwidth. The UWB-MIMO antenna system's operational band is robust and is not significantly influenced by phase variations in the other ports' excitation.

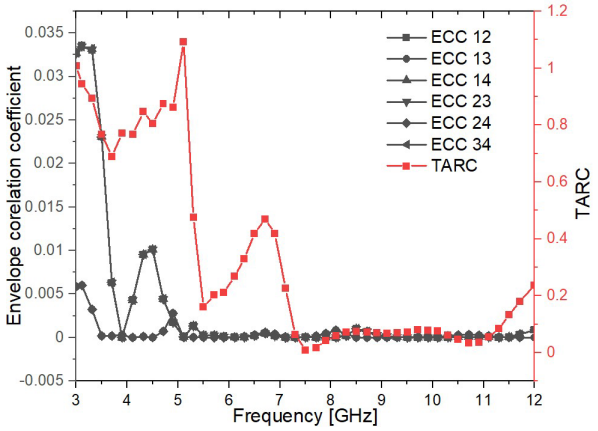

Figure 10. TARC and ECC of the quad-port UWB-MIMO antenna.

Additionally, the mean effective gain (MEG), channel capacity loss (CCL), and the envelope correlation coefficient (ECC) are important characteristics that determine the performance of a MIMO antenna [4]. All elements are represented by MEGs, which measure the average signal strength received by each. MEGs are calculated by dividing the average received power by the average incident power, defined using Equation (7). Table 2 presents the numerical results for quad-port.

$$MEG_i = 0.5\mu_{irad} = 0.5\left(1 - \sum_{j=1}^{K} |S_{ij}|\right) \tag{7}$$

Table 2. Mean effective gain of the proposed UWB-MIMO antenna.

Freq. [GHz]	Mean Effective Gain (dB)			
	Ant-1	Ant-2	Ant-3	Ant-4
4	−7.734	−7.733	−7.734	−7.734
6	−6.560	−6.560	−6.560	−6.560
8	−6.471	−6.472	−6.471	−6.471
10	−6.292	−6.293	−6.293	−6.293

where i is the antenna under observation, k the number of antennas, and μ_{irad} the radiation efficiency. For optimal diversity performance, the practical standard is that MEG should be $-3 \leq \text{MEG(dB)} < -12$, which is validated for all MIMO antennas in the proposed design.

Theoretically, adding more antennas to a MIMO system can boost its potential capacity. However, the MIMO system's channel capacity will be decreased due to uncorrelated Rayleigh fading. The capacity loss (C_{loss}) of a quadport MIMO antenna can be determined using the following equation [31, 32]:

$$C_{loss} = -\log 2 \det\left(\psi^R\right) \tag{8}$$

where (ψ^R) is the correlation matrix between the receiving antennas as defined by

$$\psi^R = \begin{vmatrix} \rho_{11} & \rho_{12} & \rho_{13} & \rho_{14} \\ \rho_{21} & \rho_{22} & \rho_{23} & \rho_{24} \\ \rho_{31} & \rho_{32} & \rho_{33} & \rho_{34} \\ \rho_{41} & \rho_{42} & \rho_{43} & \rho_{44} \end{vmatrix} \tag{9}$$

$\rho_{ij} = -|\sum_{n=1}^{4} S_{in}^* S_{nj}|$, and $\rho_{ii} = 1 - |\sum_{n=1}^{4} S_{in}^* S_{ni}|$, for $i, j = 1, 2, 3$, or 4. The proposed MIMO antenna's simulated losses are displayed in Fig. 11; it can be observed that the channel capacity loss is less than 0.02 bits/s/Hz in the operating band except 5 GHz.

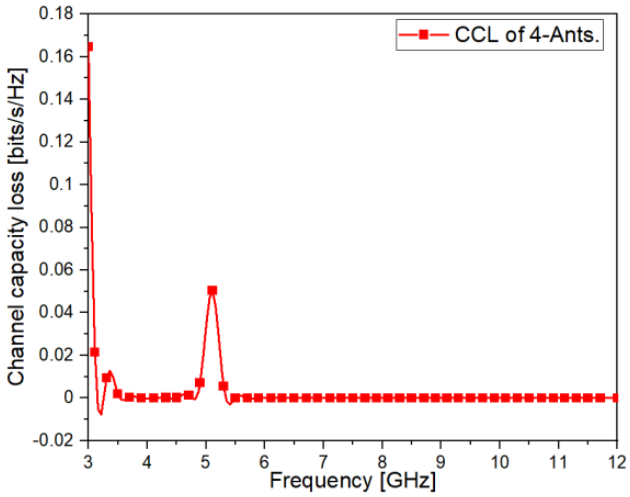

Figure 11. Channel capacity loss.

ECC defines the degree of decoupling between the antenna elements. The lower the ECC value is, the greater the diversity gain is. ECC levels less than 0.5 are considered acceptable for MIMO antennas. The correlation coefficient ρ_e can be calculated using the formula from the three-dimensional radiation

pattern [4].

$$\rho_e = \frac{\left|\int_0^{2\pi}\int_0^{\pi}\left(XPRE_{\theta i}E^*_{\theta j}P_\theta + E_{\emptyset i}E^*_{\emptyset j}P_\emptyset\right)d\Omega\right|^2}{\int_0^{2\pi}\int_0^{\pi}\left(XPRE_{\theta i}E^*_{\theta i}P_\theta + E_{\emptyset j}E^*_{\emptyset i}P_\emptyset\right)d\Omega \times \int_0^{2\pi}\int_0^{\pi}\left(XPRE_{\theta j}E^*_{\theta j}P_\theta + E_{\emptyset j}E^*_{\emptyset j}P_\emptyset\right)d\Omega} \tag{10}$$

where XPR represents the cross-polarization ratio; i and j are port numbers; and $P_\emptyset$ and P_θ are the phi and theta components of the angular diversity function. Before estimating the ECC from far-field radiation patterns, Fig. 12 plots 3D-radiation patterns at 8 GHz while exciting ports1–4. The graphic demonstrates that elements have polarization variety, with element 1 having nulls in the direction where others have the highest radiations and element 2 having nulls in the direction where others have the greatest radiations. The sun-correlated patterns result in low ECC values, which guarantees that the antenna operates efficiently in densely populated areas. Fig. 10 plots ECC values over the whole frequency range to demonstrate this. As illustrated, the ECC values for the proposed design are less than 0.1 in a uniform scattering environment between 3 and 12 GHz, indicating that the antenna radiates the most of the input power, and only a negligible portion of it is lost in coupling with other ports of the antenna.

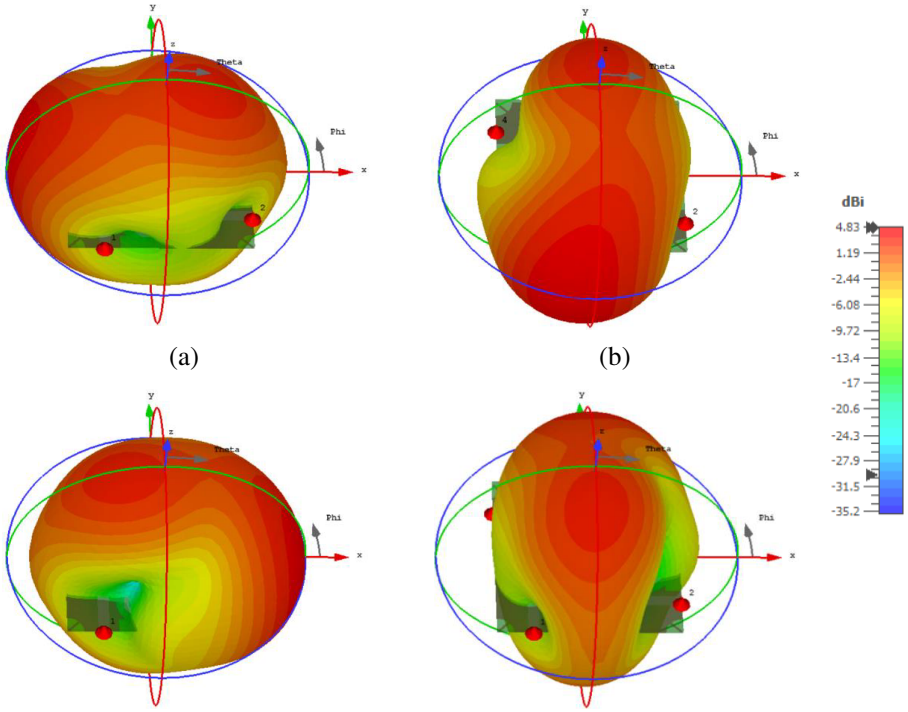

Figure 12. Three-D radiation pattern for quad-port at 8 GHz, (a) Ant.1, (b) Ant.2, (c) Ant.3, (d) Ant.4.

3.3. Radiation Pattern

The polarization diversity is explained with the help of simulated and measured two-dimensional radiation patterns in the E- and H-planes for frequencies of 4, 5, 8, and 10 GHz, as shown in Fig. 13. The figure demonstrates that the characteristics of the E-plane at higher frequencies are nearly identical to those of low frequencies. Cross-polarizations are minor in comparison to E-plane co-polarizations at the four sample frequencies. However, the discrepancies between co- and cross-polarizations are

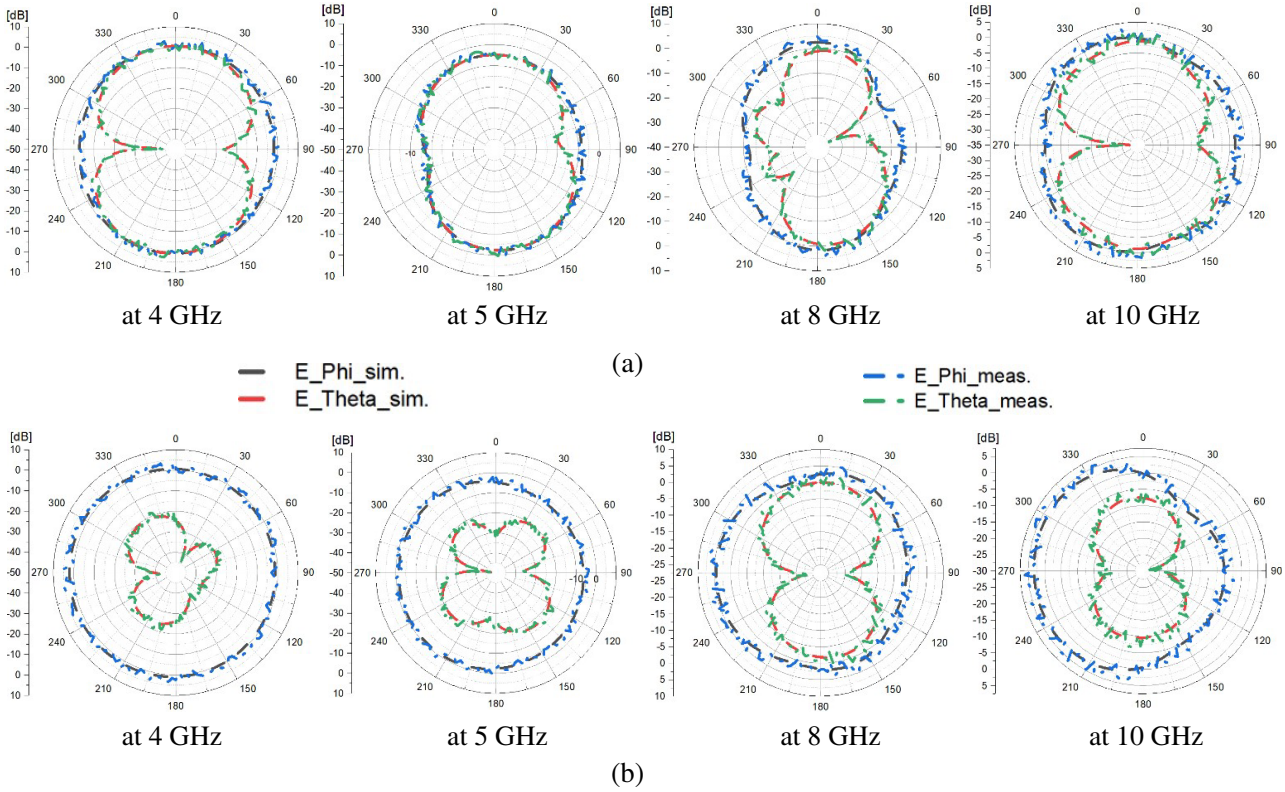

Figure 13. 2-D radiation pattern simulated and measured in xz and yz plane, (a) E-plane, (b) H-plane.

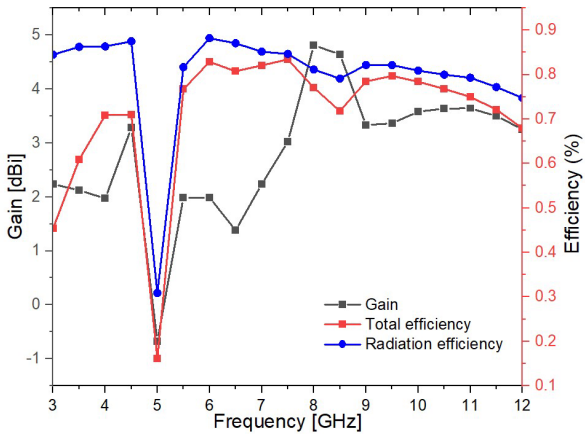

Figure 14. Gain and total/radiation efficiency of the proposed antenna.

considerable, indicating a good E-plane radiation pattern. Further, the H-plane co-polarizations are quasi-omnidirectional, whereas the cross-polarization is smaller for the frequencies. Besides, the differences are significant, resulting in a stable radiation pattern in the H-plane. Moreover, the notched band at the 5 GHz band has a lower gain than other sample frequencies.

Antenna gain is also related to radiation characteristics. It describes how much an input power's amplitude is concentrated and expanded, which means the antenna's ability to send and receive signals in a certain direction. Fig. 14 shows the changes of the simulated peak gain from 1.5 to 4.8 dBi for 3–12 GHz impedance bandwidth except for the notched band. Moreover, it is poor at low frequencies (< 4.5 GHz) because of the element's small size. However, the peak gain of higher-order modes is greatly

boosted because radiation modes become partially orientated at higher frequencies.

Figure 14 shows the antenna peak gain and total efficiency. Again, the peak gain and total efficiency exhibit band-notched features in line with previous findings. Additionally, the efficiency is greater than 75% across the full impedance bandwidth (3–12 GHz) except for the notched band at 5.5–12 GHz and drops to 60% only at the lower narrow frequency band (< 4.5 GHz), showing the UWB-MIMO antenna's excellent efficiency.

3.4. Performance Comparison with Previous Works

Employing Table 3, we compare the proposed extended UWB-MIMO antenna with published works on UWB-MIMO antenna applications. While the comparison is not exhaustive, it comes close to describing the current state-of-the-art UWB-MIMO antenna technology. The comparison findings demonstrate that the presented antenna provides an acceptable trade-off among size, isolation, bandwidth, radiation pattern, gain, MIMO diversity (TARC, MEG, ECC, and CCL), band-notched characteristics, and element number. The notch frequency (5 GHz) was eliminated in the given MIMO antenna by placing an open slot in the radiator patch in which no active elements or filter circuits are involved. Additionally, the orthogonal arrangements of the radiators improved isolation, and the monopole elements' connected ground patches provided a common reference voltage.

Table 3. Comparison with published works.

Ref.	PCB size (mm^2)	Bandwidth (GHz)	Gain (dBi)	Isolation -(dB)	No. of elements	Notched Band (GHz)	Efficiency (%)	CCL (bps/Hz)
[16]	48×48	3–11	2–4.5	< 15	4	NM	65–95	NM
[17]	45×45	2–10.6	1.8–4.2	< 17	4	5.5	NM	0.3
[18]	35×50	2–10	2.8–8.1	< 13	2	NM	93–95	
[19]	50×80	4.1–7	8	< 17	2	NM	> 80	NM
[20]	40×40	3.1–11	3.28	< 15	4	NM	NM	< 0.4
[21]	93×47	3.1–10.6	3–3.5	< 20	2	NM	80–90	NM
[22]	64×45	2.3–10.5	1–5.5	< 15	2	3.5, 5.5, 7.5	NM	NM
[23]	36×36	3.1–11.9	3.4–4.5	< 15	4	NM	75–95	NM
[24]	48×34	3.5–10	0.9–2.9	< 20	4	NM	70–97.8	< 0.3
[25]	50×25	2–12	2–4.4	< 17	4	5.4	NM	NM
[26]	40×40	3–13.5	3.5	< 15	4	NM	> 89	< 0.25
This work	32.3×32.3	3.1–12	4.8	< 15	4	5	> 75	< 0.03

4. CONCLUSION

This paper presents a compact quad-port UWB-MIMO antenna. High performance is achieved by integrating basic approaches such as shape modification and impedance transformer to improve the bandwidth from 3.1 GHz to 12 GHz frequency range of the radiators and ground plane impedance. In addition, measurements of the prototype are used to verify important parameters of the design, and the values are within limits. The prototype measurements correspond well to the simulations. As a result of these findings, the proposed UWB-MIMO antenna has a wide impedance bandwidth (3.1–12 GHz), consistent gain (3.8), high diversity qualities, quasi-omnidirectional radiation patterns, and good isolation (< -15 dB). So the antenna under consideration could be used in UWB-MIMO wireless communication systems, particularly portable ones.

ACKNOWLEDGMENT

The authors would like to thank Mustansiriyha University (www.uomustansiriyha.edu.iq) Baghdad, Iraq for its support in the present work.

REFERENCES

1. Federal Communications Commission, "First report and order, revision of part 15 of commission's rule regarding Ultra-Wideband transmission system FCC 02-48," Washington, DC, USA, 2002.
2. Kaiser, T., F. Zheng, and E. Dimitrov, "An overview of ultra-wide-band systems with MIMO," *Proceedings of the IEEE*, Vol. 97, No. 2, 285–312, 2009.
3. Jiang, C. and L. J. Cimini, "Antenna selection for energy-efficient MIMO transmission," *IEEE Wireless Communications Letters*, Vol. 1, No. 6, 577–580, 2012.
4. Liu, L., S. W. Cheung, and T. I. Yuk, "Compact MIMO antenna for portable devices in UWB applications," *IEEE Transactions on Antennas and Propagation*, Vol. 61, No. 8, 4257–4264, 2013.
5. Bassi, M., M. Caruso, M. S. Khan, A. Bevilacqua, A. D. Capobianco, and A. Neviani, "An integrated microwave imaging radar with planar antennas for breast cancer detection," *IEEE Transactions on Microwave Theory and Techniques*, Vol. 61, No. 5, 2108–2118, 2013.
6. Capobianco, A. D., M. S. Khan, M. Caruso, and A. Bevilacqua, "3–18 GHz compact planar antenna for short-range radar imaging," *Electronics Letters*, Vol. 50, No. 14, 1016–1018, 2014.
7. Zhang, S. and G. F. Pedersen, "Mutual coupling reduction for UWB MIMO antennas with a wideband neutralization line," *IEEE Antennas and Wireless Propagation Letters*, Vol. 21, 166–169, 2015.
8. Luo, C. M., J. S. Hong, and L. L. Zhong, "Isolation enhancement of a very compact UWB-MIMO slot antenna with two defected ground structures," *IEEE Antennas and Wireless Propagation Letters*, Vol. 14, 1766–1769, 2015.
9. Tao, J. and Q. Feng, "Compact ultra-wideband MIMO antenna with half-slot structure," *IEEE Antennas and Wireless Propagation Letters*, Vol. 16, 792–795, 2016.
10. Rao J. C. and N. V. Rao, "CPW-fed compact ultra wideband MIMO antenna for portable devices," *Indian Journal of Science and Technology*, Vol. 9, No. 17, 1–9, 2016.
11. Li, H., J. Liu, Z. Wang, and Y. Z. Yin, "Compact 1×2 and 2×2 MIMO antennas with enhanced isolation for ultra-wideband application," *Progress In Electromagnetics Research C*, Vol. 71, 41–49, 2017.
12. Dabas, T., D. Gangwar, B. K. Kanaujia, and A. K. Gautam, "Mutual coupling reduction between elements of UWB MIMO antenna using small size uniplanar EBG exhibiting multiple stop bands," *International Journal of Electronics and Communications*, Vol. 93, 32–38, 2018.
13. Biswas, A. K. and U. Chakraborty, "Compact wearable MIMO antenna with improved port isolation for ultra-wideband applications," *IET Microwaves, Antennas and Propagations*, Vol. 13, No. 4, 498–504, 2019.
14. Parchin, N. O., Y. I. A. Al-Yasir, H. J. Basherlou, and R. A. Abd-Alhameed, "A closely spaced dual-band MIMO patch antenna with reduced mutual coupling for 4G/5G applications," *Progress In Electromagnetics Research C*, Vol. 101, 71–80, 2020.
15. Adam, I., H. A. Rahim, M. N. M. Yasin, and M. N. M. Nasrol, "Mutual coupling suppression in wearable MIMO antenna for on/off-body WBAN applications," *Journal of Physics Conference Series*, Vol. 1755, No. 1, 2021.
16. Mao, C.-X. and Q.-X. Chu, "Compact coradiator UWB-MIMO antenna with dual polarization," *IEEE Transactions on Antennas and Propagation*, Vol. 62, No. 9, 4474–4480, 2014.
17. Tripathi, S., A. Mohan, and S. Yadav, "A compact Koch Fractal UWB MIMO antenna with WLAN band-rejection," *IEEE Antennas and Wireless Propagation Letters*, Vol. 14, 1565–1568, 2015.
18. Chithradevi, R. and B. S. Sreeja, "A compat UWB MIMO antenna with high isolation and low correlation for wireless applications," *2017 IEEE International Conference on Antenna Innovations & Modern Technologies for Ground, Aircraft and Satellite Applications (iAIM)*, 1–4, 2017.

19. Jehangir, S. S. and M. S. Sharawi, "A miniaturized UWB biplanar yagi-like MIMO antenna system," *IEEE Antennas and Wireless Propagation Letters*, Vol. 16, 2320–2323, 2017.
20. Ali, W. A. E. and A. A. Ibrahim, "A compact double-sided MIMO antenna with an improved isolation for UWB applications," *International Journal of Electronics and Communications*, Vol. 82, 7–13, 2017.
21. Radhi, A. H., R. Nilavalan, Y. Wang , H. Al-Raweshidy, A. Eltokhy, and N. A. Aziz, "Mutual coupling reduction with a wideband planar decoupling structure for UWB-MIMO antennas," *International Journal of Microwave and Wireless Technologies*, Vol. 10, No. 10, 1143–1154, 2018.
22. Jaglan, N., G. S. Dev, T. Ekta, K. Dinesh, K. B. Kumar, and S. Shweta, "Triple band notched mushroom and uniplanar EBG structures based UWB MIMO/Diversity antenna with enhanced wide band isolation," *International Journal of Electronics and Communications*, Vol. 90, 36–44, 2018.
23. Mathur, R. and S. Dwari, "Compact 4-port UWB-MIMO slot antenna with dual polarization and low correlation for spatial diversity application," *Frequenz*, Vol. 72, No. 11, 503–509, 2018.
24. Tiwari, R. N., P. Singh, B. K. Kanaujia, and K. Srivastava, "Neutralization technique based two and four port high isolation MIMO antennas for UWB communication," *International Journal of Electronics and Communications*, Vol. 110, 1–10, 2019.
25. Khan, M. S., A. Iftikhar, R. M. Shubair, A.-D. Capobianco, S. M. Asif, B. D. Braaten, and D. E. Anagnostou, "Ultra-compact reconfigurable band reject UWB MIMO antenna with four radiators," *Electronics*, Vol. 9, No. 4, 1–9, 2020.
26. Khan, M. S., S. A. Naqvi, A. Iftikhar, S. M. Asif, A. Fida, and R. M. Shubair, "A WLAN band-notched compact four element UWB MIMO antenna," *International Journal of RF and Microwave Computer-Aided Engineering*, e22282, 2020.
27. Khan, A. A., S. A. Naqvi, M. S. Khan, and B. Ijaz, "Quad port miniaturized MIMO antenna for UWB 11 GHz and 13 GHz frequency bands," *International Journal of Electronics and Communications*, Vol. 131, 1–7, 2021.
28. Chandel, R., A. K. Gautam, and K. Rambabu, "Tapered fed compact UWB MIMO-diversity antenna with dual band-notched characteristics," *IEEE Transactions on Antennas and Propagation*, Vol. 66, No. 4, 1677–1684, 2018.
29. Sharawi, M. S., "Current misuses and future prospects for printed multiple-input, multiple-output antenna systems," *IEEE Antennas and Propagation Magazine*, Vol. 59, No. 2, 162–170, 2017.
30. Al-Gertany Kareem, Q. H., M. J. Farhan, and A. K. Jassim, "Design and analysis a frequency reconfigurable octagonal ring-shaped quad-port dual-band antenna based on a varactor diode," *Progress In Electromagnetics Research C*, Vol. 116, 235–248, 2021.
31. Manteghi, M. and Y. Rahmat-Samii, "Multiport characteristics of a wide-band cavity backed annular patch antenna for multipolarization operations," *IEEE Transactions on Antennas and Propagation*, Vol. 53, No. 1, 466–474, 2005.
32. Addepalli, T. and V. R. Anitha, "Design and parametric analysis of Hexagonal shaped mimo patch antenna for S-band, WLAN, UWB and X-band applications," *Progress In Electromagnetics Research C*, Vol. 97, 227–240, 2019.